Original Research

MR Venography of the Fetal Brain Using Susceptibility Weighted Imaging

Jaladhar Neelavalli, PhD,[1]* Swati Mody, MD,[2] Lami Yeo, MD,[3,4] Pavan Kumar Jella, MS,[1] Steven J. Korzeniewski, PhD,[3,4] Sheena Saleem, DNB, MBBS,[2] Yashwanth Katkuri, MS,[1] Ray O. Bahado-Singh, MD,[3] Sonia S. Hassan, MD,[3,4] E. Mark Haacke, PhD,[1] Roberto Romero, MD, DMed Sci,[4,5,6†] and Moriah E. Thomason, PhD[4,7]

Purpose: To evaluate the feasibility of performing fetal brain magnetic resonance venography using susceptibility weighted imaging (SWI).

Materials and Methods: After obtaining informed consent, pregnant women in the second and third trimester were imaged using a modified SWI sequence. Fetal SWI acquisition was repeated when fetal or maternal motion was encountered. The median and maximum number of times an SWI sequence was repeated was four and six respectively. All SWI image data were systematically evaluated by a pediatric neuroradiologist for image quality using an ordinal scoring scheme: 1. diagnostic; 2. diagnostic with artifacts; and 3. nondiagnostic. The best score in an individual fetus was used for further statistical analysis. Visibility of venous vasculature was also scored using a dichotomous variable. A subset of SWI data was re-evaluated by the first and independently by a second pediatric neuroradiologist. Kappa coefficients were computed to assess intra-rater and inter-rater reliability.

Results: SWI image data from a total of 22 fetuses were analyzed. Median gestational age and interquartile range of the fetuses imaged were 32 (29.9–34.9) weeks. In 68.2% of the cases (n = 15), there was no artifact; 22.7% (n = 5) had minor artifacts and 9.1% (n = 2) of the data was of nondiagnostic quality. Cerebral venous vasculature was visible in 86.4% (n = 19) of the cases. Substantial agreement (Kappa = 0.73; 95% confidence interval 0.44–1.00)) was observed for intra-rater reliability and moderate agreement (Kappa = 0.48; 95% confidence interval 0.19–0.77) was observed for inter-rater reliability.

Conclusion: It is feasible to perform fetal brain venography in humans using SWI.

Key Words: fetal imaging; pregnancy; cerebral; gradient echo; phase; veins
J. Magn. Reson. Imaging 2014;40:949–957.

FETUSES WHO SUFFER stroke in utero are at increased risk of neurodevelopmental disorders (1,2), particularly hemiplegic cerebral palsy (3,4). Fetal stroke is broadly defined as an ischemic, thrombotic or hemorrhagic event occurring between 14 weeks of gestation and the onset of labor resulting in delivery (5). While most of the magnetic resonance (MR) imaging methods used in adult stroke imaging could be applied to postnatal imaging of the neonates, methodologies for evaluating and studying fetal stroke in utero are limited due to constraining factors specific to fetal imaging (6). Blood oxygen level dependent (BOLD) based signal changes in MR susceptibility weighted imaging (SWI) have been used previously in evaluating and studying stroke not only in adults, but also in pediatric (7,8) and neonatal populations (9–11). SWI has also been used in studying traumatic brain injury in the pediatric population due to its sensitivity to hemorrhagic lesions (12–15). SWI is a high resolution, fully flow compensated MR imaging technique, which is more sensitive than the typical T2* based BOLD acquisition because of its unique combination of the T2* weighted magnitude data with the

[1]Department of Radiology, Wayne State University, Detroit, Michigan, USA.
[2]Department of Pediatric Imaging, Children's Hospital of Michigan, Detroit, Michigan, USA.
[3]Department of Obstetrics and Gynecology, Wayne State University School of Medicine, Detroit, Michigan, USA.
[4]Perinatology Research Branch, Program for Perinatal Research and Obstetrics, Division of Intramural Research, Eunice Kennedy Shriver National Institute of Child Health and Human Development, NIH, Bethesda, Maryland, and Detroit, Michigan, USA.
[5]Department of Obstetrics and Gynecology, University of Michigan, Ann Arbor, Michigan, USA.
[6]Department of Epidemiology and Biostatistics, Michigan State University, East Lansing, Michigan, USA.
[7]Merrill Palmer Skillman Institute for Child and Family Development, Department of Pediatrics, Wayne State University, Detroit, Michigan, USA.
[†]R. Romero has contributed to this work as part of his official duties as an employee of the United States Federal Government.
Contract grant sponsor: NHLBI; Contract grant number: 1R42HL112580-01A1; Contract grant sponsor: Perinatal Research Initiative of the Wayne State University School of Medicine, Detroit, Michigan.
*Address reprint requests to: J.N., University Health Center, 4201 St. Antoine, 5E-12, Detroit, MI 48201. E-mail: jaladhar@wayne.edu
Received January 18, 2013; Accepted September 4, 2013.
DOI 10.1002/jmri.24476
View this article online at wileyonlinelibrary.com.

phase data (16,17). Phase image from gradient echo sequences like SWI provides distinctive contrast, different from the conventional T1, T2, and T2* contrast, accentuating small differences in tissue magnetic susceptibility property. Because of this, SWI is used in distinguishing arteries from veins (18–20), is sensitive to microbleeds (16,21) and to changes in venous oxygen saturation (22–25) and has also been used to quantify cerebral venous oxygen saturation (26). In a stroke, increased oxygen extraction in the tissue with reduced perfusion leads to an increase in deoxyhemoglobin content in the veins and could lead to their prominent appearance on SWI (25,27). Unusually prominent deep medullary veins have been identified on SWI in hypoxic ischemic injury (HII) in neonates (10). Kitamura et al reported neonates with HII with a normal appearance of deep medullary veins on SWI are more likely to have normal neurologic outcomes compared to patients with prominent deep medullary veins (10).

Given the sensitivity of SWI as a venographic technique, its utility in evaluating stroke in adult, pediatric and neonatal populations and its potential for quantitative evaluation of blood oxygenation, we anticipate that SWI may be an important tool in fetal brain imaging as well, especially for studying and imaging hypoxic ischemic injury. Hence, the purpose of this work was to evaluate the feasibility of performing venography of the fetal brain using SWI. Specifically, we adapted clinically available SWI sequence for fetal brain imaging, applied it to imaging normal fetuses and evaluated the quality of the acquired images.

MATERIALS AND METHODS

Study Population

Twenty-two pregnant women with singleton pregnancies between 18 to 38 years and 19 and 40 weeks of gestation, who were receiving care at the Hutzel Women's Hospital in Detroit, MI, USA were non-consecutively recruited. Women with uncomplicated pregnancies, a normal ultrasound examination and reporting no contraindications for MRI were eligible to participate. The study was approved by the local institutional review board and was compliant with HIPAA. Written informed consent was obtained before the MRI scan. No sedation was used for fetal MRI scan. Study participants were followed longitudinally to assure that they did not develop complications during pregnancy. The median gestational age of the fetuses included was 32 weeks with the interquartile range of 29.9 to 34.9 weeks.

MR Imaging Protocol

Three of the women were scanned on a 1.5 Tesla (T) GE Signa system (Milwaukee, WI) and the remaining (n = 19) on a 3.0T Siemens Verio system (Erlangen, Germany).

Imaging at 1.5T

An eight-channel cardiac array with spine receive coils were used for imaging. Normal anatomical data were acquired using a T2 weighted single shot fast spin echo (SSFSE) technique with repeat time (TR) between 1192 and 1240 milliseconds (ms), echo time (TE) 242 ms, slice thickness of 4 mm, voxel size 1.13 × 1.13 mm^2, flip angle of 90° and acquisition matrix size of 256 × 160. Fetal SWI sequence was implemented by modifying the imaging parameters of a two-dimensional (2D) multiecho, fast spoiled gradient echo sequence with flow compensation. The sequence was modified to save both magnitude and phase data. The following sequence parameters were used: TR = 80 to 105 ms, TEs = 8.4, 16.8, 25.3, 33.7 ms, slice thickness of 5 or 6 mm, flip angle 18°, field of view (FOV) 350 × 350 mm^2, acquisition matrix size of 512 × 256, giving an acquisition voxel size of 0.7 × 1.4 × 5 mm^3. A parallel imaging factor of 2 in phase encoding direction was used. Images were interpolated to a matrix size of 512 × 512, with an apparent voxel size of 0.7 × 0.7 mm^2 in-plane. The sequence was implemented in a multi breath-hold mode and the total data acquisition time depended on the number of slices acquired. Imaging time for acquiring two slices was typically between 24 and 26 s. Volume coverage was achieved by acquiring multiple slices in a multi breath-hold mode with a total acquisition time for 12 slices of approximately 2.5 min.

Imaging at 3.0T

A six-channel body flex array coil with the spine receive coil were used for imaging. Anatomical data were acquired using a T2-weighted single shot turbo spin echo sequence with half-Fourier reconstruction (HASTE sequence) using the following parameters: TR 3000 ms, TE 140 ms, slice thickness 3 mm, voxel size of 0.87 × 0.87 mm^2 in-plane, flip angle 75° and an acquisition matrix of 320 × 320. Imaging parameters of the conventional SWI sequence were modified for the fetal imaging application for fast data acquisition. Both two and three dimensional (2D and 3D) data acquisition versions the SWI sequence were implemented for fetal brain imaging as described below. For 2D fetal SWI, a 2D spoiled gradient echo imaging sequence with flow compensation in all three directions and TR of 250 to 280 ms, TE between 17 to 19 ms, slice thickness of 3 or 3.5 mm, voxel size of 0.78 × 1.56 mm^2 in-plane, flip angle 32°, a parallel imaging factor of 2 along phase encoding direction, and an acquisition matrix size of 448 × 168 was implemented. Images were interpolated to 0.78 × 0.78 mm^2 in-plane resolution. A total of 10 or 11 slices were collected within an acquisition time of 22 to 24 s. For 3D fetal SWI, a 3D spoiled gradient echo sequence with flow compensation in all three directions and TR between 20 and 23 ms, TE between 13 and 17.3 ms, slice thickness of 3 or 3.5 mm, voxel size 0.78 × 1.56 mm^2 in-plane, flip angle 10, and an acquisition matrix size of 448 × 175 was implemented. Reconstructed images were interpolated by zero filling to 0.78 × 0.78 mm^2 in-plane resolution. A total of 16 slices were acquired and total data acquisition time was approximately 22 to 24 s. Both 2D and 3D SWI sequence at 3.0T were applied under maternal breath-hold condition.

Table 1
MR Imaging Parameters for Fetal SWI

Sequence mode	TR(ms)	TE(ms)	In plane reconstructed voxel size (mm)	Slice thickness (mm)	BW (Hz/pixel)	No. of slices
			1.5T (GE Signa)			
2D	100 or 105	33.7	0.7 x 0.7	5 to 6 mm	122	12
			3T (Siemens Verio)			
2D	250 to 280	17 to 19	0.78 x 0.78	3 to 3.5 mm	199	11
3D	20 to 23	13.5 to 17.3	0.78 x 0.78	3 to 3.5 mm	219	16

Except for the cases where fetal motion precluded it, SWI data was acquired in axial orientation relative to the fetal brain. The 2D SWI sequence was applied in all but one fetal MR scan (n = 21); whereas, 3D-SWI data were collected only in a few fetal scans when total scan time restrictions permitted (n = 15). Magnitude and phase images obtained from these SWI sequences were processed as described in Haacke et al (19) to obtain the SWI image data. Table 1 summarizes the key imaging parameters of the fetal SWI sequences. In most fetal scans, SWI data acquisition (2D and/or 3D) was repeated when motion was encountered. This repeated image acquisition is common place in clinical fetal imaging (28). The median number of times an SWI acquisition (2D and/or 3D) was repeated in a fetus was four with a maximum of six, which was in only one fetus.

Data Evaluation

All SWI image data (henceforth referred to as SWI data) from the fetal scans were evaluated for image quality using an ordinal quality scoring scheme by a pediatric neuroradiologist (S.M.) with 12 years of experience. Specifically, image quality assessment was focused on the fetal brain region only as that is the region of investigation in this study. The ordinal scoring criteria for image quality is given in Table 2. Images of diagnostic quality with good magnitude definition and no artifacts were given the score of 1. Image volumes with minor artifacts but still of diagnostic quality were scored as 2. Images of nondiagnostic quality with poor magnitude definition and major artifacts were scored as 3. Both 2D and 3D SWI data were scored individually for image quality. Because multiple 2D and/or 3D SWI data were often acquired in one fetal scan, an overall SWI data quality score was then determined for that particular fetus by taking the minimum of the scores of all SWI scans for that fetus. Furthermore, the SWI dataset receiving the optimal score was then evaluated for visibility of cerebral venous vasculature using a dichotomous, Yes (1) >No (0) classification by the same pediatric neuroradiologist (S.M.). A value of 1 was assigned when veins in deep white matter or cortical veins were visible; otherwise 0 was assigned. Because the SWI scan volume covered slightly different regions of the brain for different fetuses, due to limited volume coverage and different fetal brain sizes, evaluation of visibility of a single common venous structure across all fetuses was not feasible.

Of the 22 fetuses scanned, 19 were randomly chosen for evaluating intra-rater and inter-rater agreements. The quality of the SWI data acquired from this subset of fetuses was reviewed and scored using the same ordinal scale as described above, in a blinded manner by another neuroradiologist for inter-rater agreement evaluation. The scoring of this subset of fetal SWI data was repeated by the first neuroradiologist (S.M.) with a gap of 6 months between the first and the second reviews for intra-rater agreement evaluation. For each reviewer, the overall SWI data quality score, obtained by taking the minimum of the scores of all SWI scans for an individual fetus, was used for further statistical analysis. This process of considering the best image volume of the available scan data is similar to the image review process in clinical fetal imaging, where sequences are repeated until images without fetal motion are obtained and the best quality scan data is used for diagnostic purposes. Cichetti-Allison weighted kappa coefficients were calculated as a measure of inter- and intra- rater agreement. A priori classifications of Kappa coefficients were as follows: "0" as indicating no agreement; "0–0.20" as slight agreement; "0.21–0.40" as fair agreement, "0.41–0.60" as moderate agreement; "0.61–0.80" as substantial agreement; and "0.81–1.0" as near perfect agreement. A 5% threshold for type I error was used to determine statistical significance. Statistical analyses were performed using SAS version 9.3 (Cary, NC).

RESULTS

Representative examples of the SWI data are shown in Figure 1. The phase signature of the veins, due to

Table 2
Ordinal Scoring Scheme for Image Quality Assessment

Quality scoring index		
Score	Interpretation	No. of datasets receiving the score
1	Diagnostic quality images with good magnitude definition and no artifacts.	n = 15
2	Minor artifacts being present but overall image volume is still of diagnostic quality.	n = 5
3	Non-diagnostic images with very poor magnitude definition and containing major artifacts.	n = 2

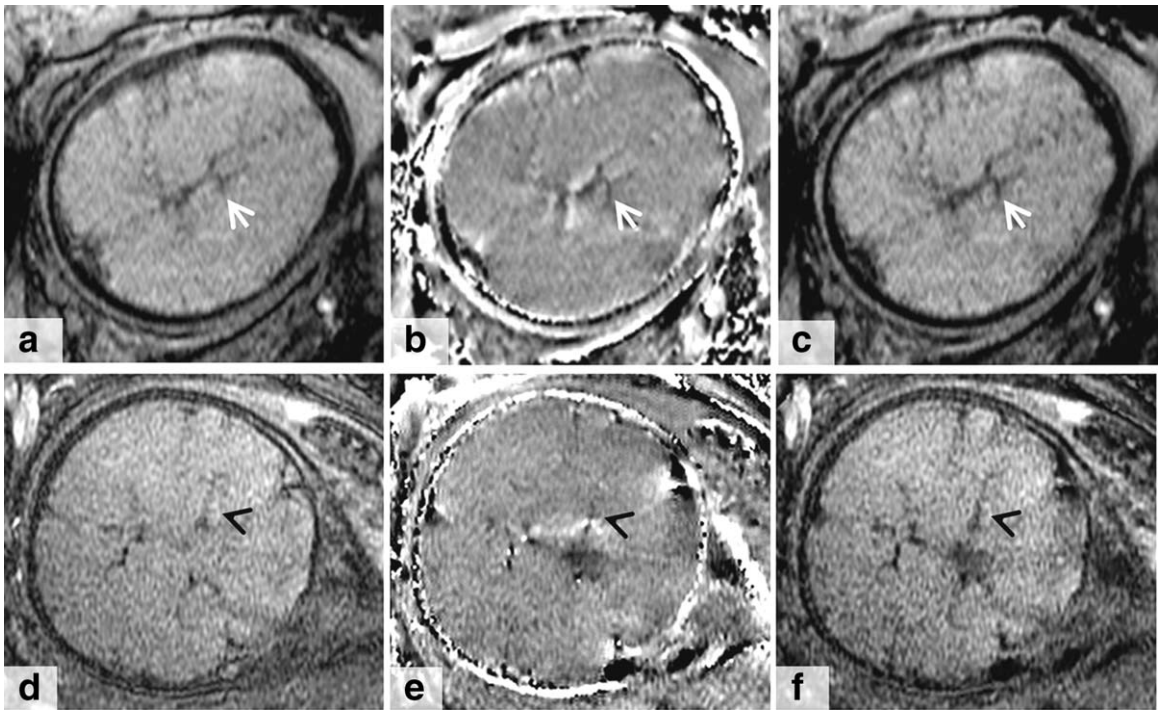

Figure 1. Susceptibility weighted images of the fetal brain. Top Row: Images were acquired in axial orientation relative to the fetus using a 3D SWI sequence at 3.0T field strength from a fetus at 36 3/7 weeks of gestation. Bottom Row: Images were acquired in coronal orientation relative to the fetus using a 2D SWI sequence at 1.5T field strength from a fetus at 35 3/7 weeks of gestation. **a,d:** Original magnitude images. **b,e:** Corresponding filtered phase images. **c,f:** Corresponding susceptibility weighted magnitude image (SWI image). Veins are already seen to some extent in the original magnitude images **(a,d)** due to T2* signal loss; white arrow head in **(a)** indicating the thalamostriate vein. Phase images in **(b,e)** also show the veins with their characteristic phase signature. After applying the mask generated using this phase information to the corresponding original magnitude images, processed SWI images in **(c,f)** clearly improve the vessel contrast (white arrow in **(a)** and black arrow head in **(f)**). Imaging resolution corresponding to the scan in the top row (3.0T - 2D SWI) was $0.78 \times 1.5 \times 3$ mm^3 (reconstructed to 0.78×0.78 mm^2 in-plane) and $0.7 \times 0.1.4 \times 5$ mm^3 (reconstructed to 0.7×0.7 mm^2 in-plane) for the bottom row (1.5T - 2D SWI).

their paramagnetic nature, is clearly visible in the images (Figs. 1b,e) and helps in enhancing magnitude contrast after SWI processing (Figs. 1c,f) (29,30). Of SWI data reviewed from 22 fetuses, 68.2% (n = 15) was found to be of diagnostic quality with no artifacts and received the optimal score of 1. Minor artifacts were seen in 22.7% (n = 5) of the cases which were still of diagnostic quality and received a score of 2. In 9.1% (n = 2) of the cases, images were of nondiagnostic quality and received a score of 3 due to severe artifacts resulting either from fetal motion, small imaging FOV or bulk susceptibility artifacts from air–tissue or bone–tissue interface. These results are summarized in Table 2. SWI data, which received a score of 2, typically had coil drop-off (ie, varying signal to noise ratio (SNR), from high to low across the image), artifacts from a small FOV or susceptibility related artifacts. Examples of the typical artifacts seen in the

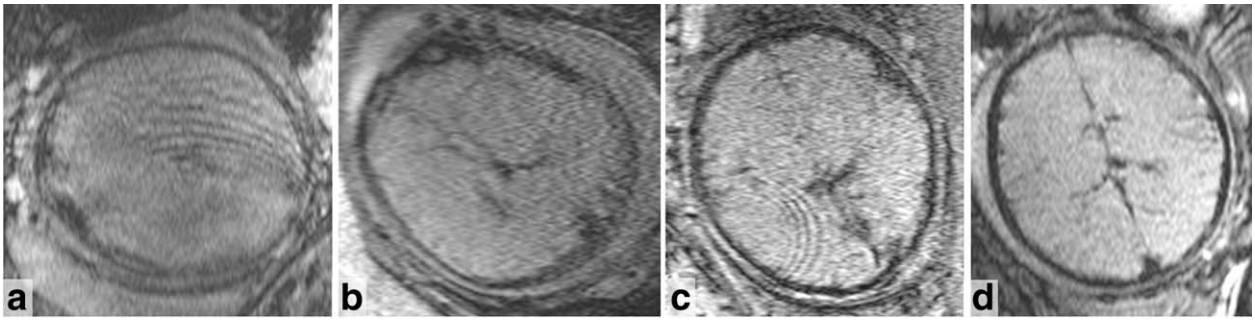

Figure 2. Unprocessed SWI magnitude images illustrating typical image quality and artifacts seen and their respective scores. **a:** Image containing fetal motion artifact and an artifact due to small FOV; score 3. **b:** Image with varying signal to noise ratio across the fetal brain region. This is due to insufficient reference lines required for image reconstruction with parallel imaging; score −2. **c:** Another image with score 2, containing what appears as a ripple artifact in one part of the fetal brain. This artifact is due to signal contamination from tissue outside the small field of view; score 2. **d:** Fetal image with visibly no artifacts in the fetal brain region; score 1.

Table 3
Intra-rater Reliability*

	Rater-1 - Time 2			
Rater-1 – Time 1	1 - Diagnostic quality images without any artifacts	2 - Diagnostic quality images with some artifacts	3- Nondiagnostic quality images	Total
1 - Diagnostic quality images without any artifacts	10	0	0	10
2 - Diagnostic quality images with some artifacts	3	5	0	8
3- Nondiagnostic quality images	0	0	1	1
Total	13	5	1	19

*In a subset of cases fetal brain SWI data quality was assessed a pediatric neuroradiologist twice with a 6-month gap between the first and second assessment.

images with their corresponding scores are shown in Figure 2.

SWI data from 19 fetuses were assessed twice by a single rater to estimate intra-rater reliability and once more by an additional rater to assess inter-rater reliability. Overall, substantial intra-rater agreement was observed (Kappa = 0.73; 95% confidence interval 0.44–1.00). As shown in Table 3, discrepancies within repeated assessments by rater-1 included three datasets that were first graded as diagnostic quality with some artifacts and were later considered to be of diagnostic quality without any artifacts. As shown in Table 4, moderate agreement (Kappa = 0.48; 95% confidence interval 0.19–0.77) was observed for inter-rater reliability. Eight images classified as diagnostic quality without any artifacts by rater-1 were classified by rater-2 as having some artifacts (n = 7) or being of nondiagnostic quality (n = 1). Additionally, one image classified by rater-2 as nondiagnostic quality (score = 3) received a diagnostic quality with artifacts rating (score = 2) by rater-1. However, when only a binary classification of diagnostic quality versus nondiagnostic quality was considered, agreement was greater than that observed for the three category classifications: 100% intra-rater agreement (agreed on 19/19), and 90% inter-rater agreement (agreed on 17/19).

Cerebral venous vasculature was visible in 86.4% (n = 19) of the cases, and in 100% of those imaged after 32 weeks of gestation (n = 10). Figure 3 illustrates the proportion of cases in which venous vasculature was visible by gestational age interval. Minimum intensity projection SWI images from different fetuses at different gestational ages are shown in Figure 4. This collage illustrates the different extent of venous vasculature visualized on SWI as the gestational age progresses. Finally, Figure 5 demonstrates in detail the venous vasculature in a fetus at 37 1/7 weeks of gestation. By comparing venous structures visualized in this fetus with what is typically seen in adult SWI venography, major veins like thalamostriate veins, internal cerebral veins, anterior septal veins, and basal vein of Rosenthal are clearly identified.

DISCUSSION

In this study, fetal brain MR venography was performed using SWI and image quality was evaluated. While venous vasculature was visible on SWI in 86.4% of the fetuses, only moderate inter-rater agreement was seen in SWI image quality. It is important to note here that, while all the SWI data acquired in an individual fetus were evaluated for data quality, only the best score obtained in an individual fetus was used for inter- and intra-rater agreement analysis. The reported data quality results are also from the best score in a given fetus. Using the best data quality rating in an individual fetus is representative of the conventional clinical fetal imaging process where acquisition for different sequences are often repeated whenever motion is encountered and the acquisition with the best data quality is then used by the radiologist for diagnostic purposes. Both SWI

Table 4
Inter-rater Reliability

	Rater-2			
Rater-1	1 - Diagnostic quality images without any artifacts	2 - Diagnostic quality images with some artifacts	3- Nondiagnostic quality images	Total
1 - Diagnostic quality images without any artifacts	5	7	1	13
2 - Diagnostic quality images with some artifacts	0	4	1	5
3- Nondiagnostic quality images	0	0	1	1
total	5	11	3	19

*In a subset of cases, fetal brain SWI data quality was assessed by a second pediatric neuroradiologist for evaluating inter-rater reliability.

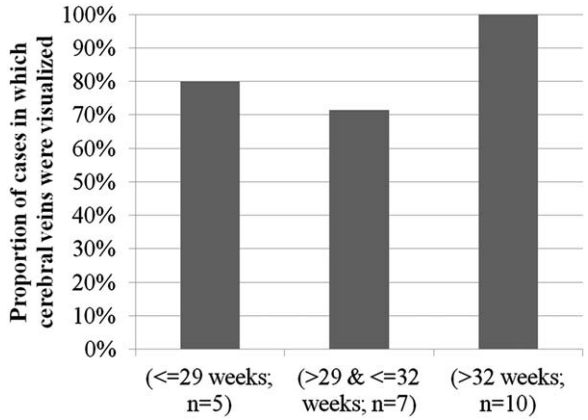

Figure 3. Proportion of cases with visible cerebral venous vasculature by gestational age at image assessment.

image quality and visibility of veins depend on many sequence parameters such as the TE, TR, flip angle, voxel size, and the number of averages. In the case of fetal imaging, an additional constraint of total imaging time is imposed. Rapid data acquisition is required for fetal imaging, mainly to minimize the effects of any maternal respiratory motion and to reduce the probability of fetal motion occurring during the scan. In this study, conventional clinical 2D and 3D SWI sequence parameters were modified to bring the total data acquisition time to between 21 and 25 s which is a typical maternal breath-hold capacity in pregnancy (31). Data acquisition matrix size (consequently the voxel size), TR, and TE were the primary experimental parameters that needed to be adjusted for the total acquisition time to be within 25 s. Flip angle was adjusted according to the changes in TR to maintain good SNR. Notably, to achieve this reduction in scan time, larger voxel sizes had to be used compared to conventional $0.5 \times 1 \times 2$ mm^3 voxel size that is typically used in a clinical adult brain SWI (32). This could adversely affect visualization of smaller veins in SWI due to partial volume effects (33). Because of the small number of fetuses in which both 2D and 3D SWI data was acquired and the number of repeat acquisitions for each differed from case to case, a statistical evaluation comparing the data quality of 2D and 3D SWI was not completed. However, a cursory comparison of the data quality scores of 2D and 3D SWI acquisitions (minimum possible score for 2D and 3D acquisitions) shows that in 12 of these 14 fetuses (85.7%), data quality of 2D SWI was equal to or better than that of 3D SWI. This is in broad agreement with what is theoretically expected based on the differences in 2D and 3D MRI data acquisition schemes. Due to the long duration over which partition (slice direction) encoding for the whole imaging volume occurs in 3D sequences, they are typically more susceptible to motion artifacts than 2D acquisition methods (34).

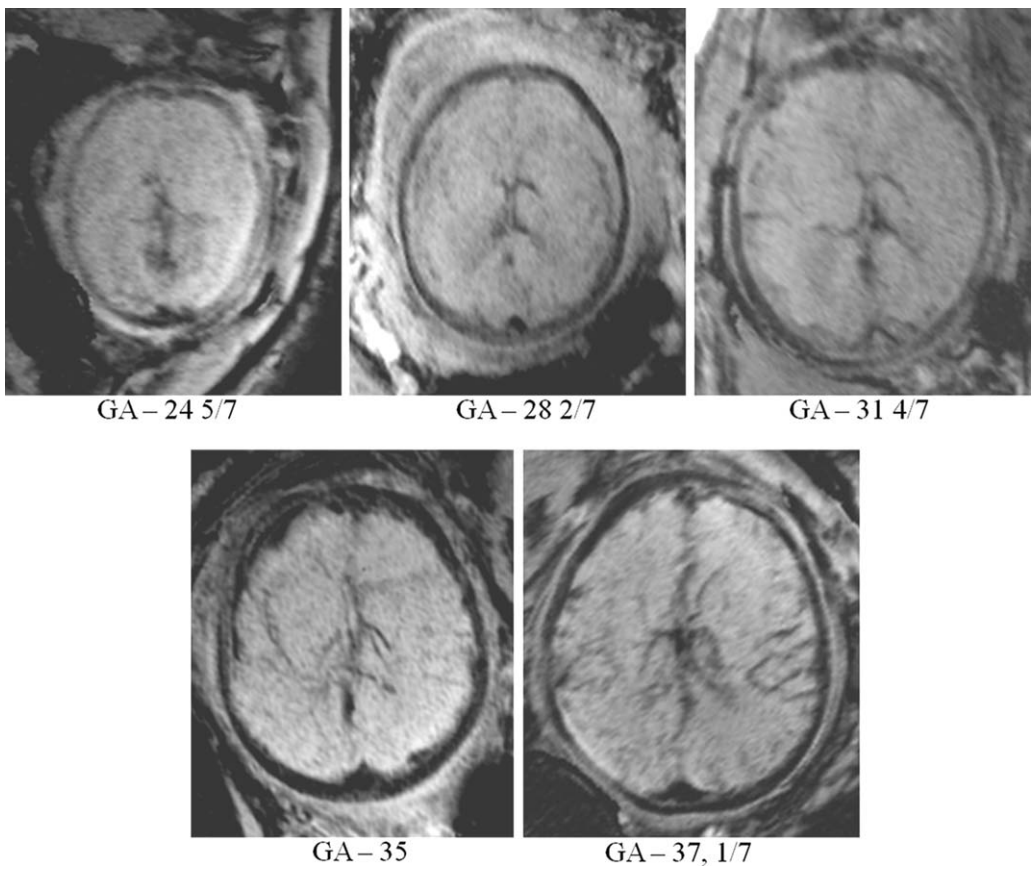

Figure 4. Fetal brain venograms generated from SWI images (minimum intensity projections). Venograms from different fetuses at different gestational ages are shown to illustrate the variation of visualized cerebral venous vasculature in the human fetus with gestational age.

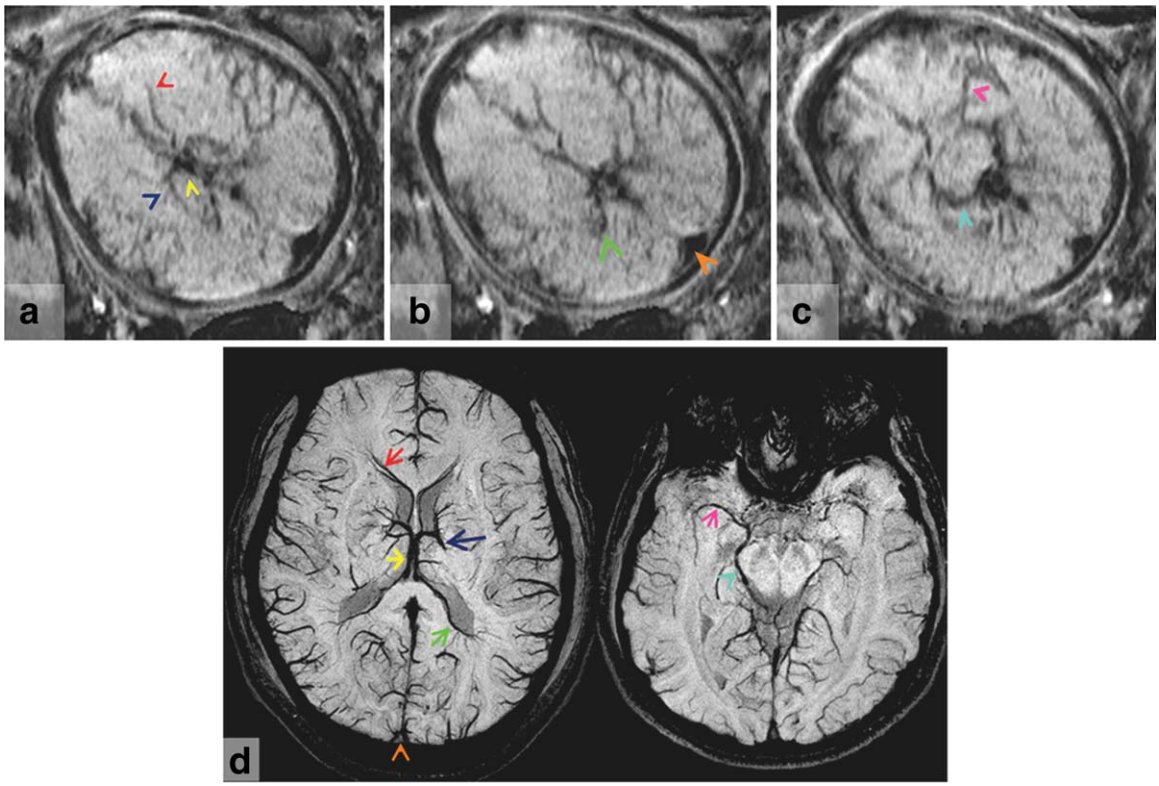

Figure 5. Venous vasculature in a 37 1/7 week fetus, identifiable based on adult venous anatomy. **a:** Septal vein (red), Thalamostriate vein (blue), Internal cerebral veins (yellow). **b:** medial atrial vein (green), superior sagittal sinus (orange). **c:** Basal vein of Rosenthal (light blue), deep middle cerebral vein (pink). Images shown here are minimum intensity projection SWI images, projected over 12 mm thickness of tissue to show contiguity of venous vasculature within. These fetal data were acquired at 3T field strength using a 3D SWI sequence. SWI images from an adult brain are shown in (**d**) for visual comparison of the venous anatomy.

Visibility of veins in SWI is dependent on the phase signature of the venous vasculature, which in-turn is a function of blood oxygenation level, blood hematocrit and the magnetic susceptibility of fetal blood (35,36). Fetal blood hematocrit changes with gestational age, increasing almost linearly from approximately 33% at 20 weeks to 43% at term (37). Oxygenation of the arterial blood supply of the fetus, by means of the umbilical vein, is also known to change with gestational age (38), which may result in a related variation in venous oxygen saturation with gestational age. Furthermore, fetal hemoglobin has a slightly different morphology that leads to its increased oxygen binding affinity compared with adult hemoglobin. Because the MR visible magnetic property of blood, namely its magnetic susceptibility, is modulated by oxygenation or de-oxygenation of hemoglobin, this difference in conformation of fetal hemoglobin with respect to adult hemoglobin, may translate to different magnetic properties (39–41) of fetal blood compared to adult blood. Cerebral blood flow rate also influences oxygen extraction fraction (35). All these factors, namely hematocrit, magnetic susceptibility of fetal blood, and blood flow can affect the net phase seen in veins. At least one of these factors, namely hematocrit if not all, is known to change with fetal gestational age. Thus, normal physiological variation in the developing venous vasculature along with gestational age may be affecting venous phase and their visibility in SWI. The variation in the extent of visible venous vasculature with gestational age illustrated in the images shown in Figure 4 supports this hypothesis. Additionally, as mentioned above, SWI sequence parameters such as TE and image resolution can influence visibility of veins (42,43). Specifically, the longer the TE the better the phase definition within the veins, and the smaller the voxel size, the better the visibility of smaller veins. Although there is some variation in the TEs used in acquisition of data, because this variation was only between 2 and 4 ms, we do not expect its influence to be significant on the variability in venous visibility in this study.

SWI requires additional postprocessing for combining magnitude and phase information. Apart from the factors mentioned above, fetal head orientation relative to the main magnetic field also influences venous phase in SWI. Hence, conventional SWI post-processing performed on MR magnet consoles is not appropriate for fetal SWI. This problem was overcome in this study by appropriately modulating the phase mask generation step (29,44) to account for arbitrary head orientation. Specifically, linear phase mask with appropriate sign for enhancing venous vasculature was chosen depending on the sign of the venous phase. Recently developed post-processing methods (45), which are independent of fetal head orientation could also alleviate this problem. However, higher resolution data would be required for the optimal

application of this methodology. Artifacts related to the small FOV, fetal motion and susceptibility effects from air–tissue or bone–tissue interface affected the SWI image quality in this study. Artifacts related to the small FOV refer to aliasing artifacts arising from signal contributions from outside the FOV which were seen to disappear when a larger FOV was used for imaging. These artifacts can be avoided using outer-volume suppression (or reduced FOV) techniques, which allow precise excitation of a small region of interest within a larger object (46,47). These reduced FOV imaging techniques could also be used to achieve higher spatial resolution. In conjunction with reduced FOV imaging, novel sampling and reconstruction schemes like segmented echo planar imaging could provide a factor 3 to 5 decrease in data acquisition time (48). For a fixed imaging time, such schemes could further be used for obtaining higher resolution data which can further improve image quality and visualization of veins in SWI.

There are a few limitations to this study. Although fetal SWI data from 1.5T and 3T was evaluated, due to the small number of fetal scans at 1.5T, comparison could not be made between image quality and venous visibility at 1.5T versus 3.0T. Similarly, because 3D SWI was not acquired in all cases, a comparision of data quality and visibility of veins between 3D versus 2D fetal SWI were not carried out. A key aspect in this study is that without any pulse sequence modification, conventional, clinically available sequences were modified to obtain fetal SWI data. Despite this, data from only 31.8 % ($n = 7$) of the cases contained artifacts. This shows that fetal SWI data could be obtained clinically with currently available SWI sequences. However, with appropriate pulse sequence modifications using novel fast imaging techniques (46,48) the speed of data acquisition and imaging resolution can significantly be improved. Finally, the clinical value of SWI was not assessed. Future studies with SWI scan data from a larger number of normal and at-risk fetuses would be required to ascertain the clinical utility of fetal SWI. Nonetheless, a recent case report already highlights the clinical utility of SWI in imaging the fetal brain in cases of suspected intra-cerebral hemorrhage (49).

In conclusion, we have demonstrated the feasibility of performing magnetic resonance venography of the fetal brain in humans using clinically available conventional susceptibility weighted imaging sequence.

ACKNOWLEDGMENTS

This research was supported in part, by the perinatology Research Branch, Division of Intramural Research, Eunice Kennedy Shriver National Institute of Child Health and Human Development, NIH, DHHS; the STTR grant from NHLBI (1R42HL112580-01A1) and by the Wayne state university's Perinatal Research Initiative. This work was also supported in part, by Wayne State University's Perinatology Virtual Discovery Grant (made possible by W.K. Kellogg Foundation award P3018205 to J.N. and M.E.T.).

REFERENCES

1. Rees S, Harding R, Walker D. The biological basis of injury and neuroprotection in the fetal and neonatal brain. Int J Dev Neurosci 2011;29:551–563.
2. Wu YW, March WM, Croen LA, Grether JK, Escobar GJ, Newman TB. Perinatal stroke in children with motor impairment: a population-based study. Pediatrics 2004;114:612–619.
3. Himmelmann K, Ahlin K, Jacobsson B, Cans C, Thorsen P. Risk factors for cerebral palsy in children born at term. Acta Obstet Gynecol Scand 2011;90:1070–1081.
4. Bax M, Tydeman C, Flodmark O. Clinical and MRI correlates of cerebral palsy: the European Cerebral Palsy Study. JAMA 2006; 296:1602–1608.
5. Ozduman K, Pober BR, Barnes P, et al. Fetal stroke. Pediatr Neurol 2004;30:151–162.
6. Prayer D, SpringerLink (Online service). Fetal MRI. Medical radiology diagnostic imaging. New York: London: Springer; 2011.
7. Cardenas JF, Rho JM, Kirton A. Pediatric stroke. Childs Nerv Syst 2011;27:1375–1390.
8. Altinok D, Agarwal A, Ascadi G, Luat A, Tapos D. Pediatric hemiplegic migraine: susceptibility weighted and MR perfusion imaging abnormality. Pediatr Radiol 2010;40:1958–1961.
9. Lequin MH, Dudink J, Tong KA, Obenaus A. Magnetic resonance imaging in neonatal stroke. Semin Fetal Neonat Med 2009;14: 299–310.
10. Kitamura G, Kido D, Wycliffe N, Jacobson JP, Oyoyo U, Ashwal S. Hypoxic-ischemic injury: utility of susceptibility-weighted imaging. Pediatr Neurol 2011;45:220–224.
11. Niwa T, de Vries LS, Benders MJ, Takahara T, Nikkels PG, Groenendaal F. Punctate white matter lesions in infants: new insights using susceptibility-weighted imaging. Neuroradiology 2011;53:669–679.
12. Tong KA, Ashwal S, Holshouser BA, et al. Diffuse axonal injury in children: clinical correlation with hemorrhagic lesions. Ann Neurol 2004;56:36–50.
13. Ashwal S, Babikian T, Gardner-Nichols J, Freier MC, Tong KA, Holshouser BA. Susceptibility-weighted imaging and proton magnetic resonance spectroscopy in assessment of outcome after pediatric traumatic brain injury. Archives of physical medicine and rehabilitation 2006;87(Suppl 2):S50–S58.
14. Babikian T, Freier MC, Tong KA, et al. Susceptibility weighted imaging: neuropsychologic outcome and pediatric head injury. Pediatr Neurol 2005;33:184–194.
15. Tong KA, Ashwal S, Holshouser BA, et al. Hemorrhagic shearing lesions in children and adolescents with posttraumatic diffuse axonal injury: improved detection and initial results. Radiology 2003;227:332–339.
16. Mori N, Miki Y, Kikuta K, et al. Microbleeds in moyamoya disease: susceptibility-weighted imaging versus T2*-weighted imaging at 3 Tesla. Invest Radiol 2008;43:574–579.
17. Sehgal V, Delproposto Z, Haddar D, et al. Susceptibility-weighted imaging to visualize blood products and improve tumor contrast in the study of brain masses. J Magn Reson Imaging 2006;24: 41–51.
18. Wang Y, Yu Y, Li D, et al. Artery and vein separation using susceptibility-dependent phase in contrast-enhanced MRA. J Magn Reson Imaging 2000;12:661–670.
19. Haacke EM, Xu Y, Cheng YC, Reichenbach JR. Susceptibility weighted imaging (SWI). Magn Reson Med 2004;52:612–618.
20. George U, Jolappara M, Kesavadas C, Gupta AK. Susceptibility-weighted imaging in the evaluation of brain arteriovenous malformations. Neurol India 2010;58:608–614.
21. Gao T, Wang Y, Zhang Z. Silent cerebral microbleeds on susceptibility-weighted imaging of patients with ischemic stroke and leukoaraiosis. Neurol Res 2008;30:272–276.
22. Hermier M, Nighoghossian N. Contribution of susceptibility-weighted imaging to acute stroke assessment. Stroke 2004;35: 1989–1994.
23. Yamashita E, Kanasaki Y, Fujii S, Tanaka T, Hirata Y, Ogawa T. Comparison of increased venous contrast in ischemic stroke using phase-sensitive MR imaging with perfusion changes on

flow-sensitive alternating inversion recovery at 3 Tesla. Acta Radiol 2011;52:905–910.
24. Viallon M, Altrichter S, Pereira VM, et al. Combined use of pulsed arterial spin-labeling and susceptibility-weighted imaging in stroke at 3T. Eur Neurol 2010;64:286–296.
25. Kesavadas C, Santhosh K, Thomas B. Susceptibility weighted imaging in cerebral hypoperfusion-can we predict increased oxygen extraction fraction? Neuroradiology 2010;52:1047–1054.
26. Haacke EM, Tang J, Neelavalli J, Cheng YC. Susceptibility mapping as a means to visualize veins and quantify oxygen saturation. J Magn Reson Imaging 2010;32:663–676.
27. Kesavadas C, Thomas B, Pendharakar H, Sylaja PN. Susceptibility weighted imaging: does it give information similar to perfusion weighted imaging in acute stroke? J Neurol 2011;258:932–934.
28. Brugger PC, Prayer D. Actual imaging time in fetal MRI. Eur J Radiol 2012;81:E194–E196.
29. Haacke EM, Reichenbach JR. Susceptibility weighted imaging in MRI : basic concepts and clinical applications. Hoboken, NJ: Wiley-Blackwell; 2011. xvi, 743.
30. Sehgal V, Delproposto Z, Haacke EM, et al. Clinical applications of neuroimaging with susceptibility-weighted imaging. J Magn Reson Imaging 2005;22:439–450.
31. McMechan FH. The diagnostic and prognostic value of breath-holding test. Cal State J Med 1922;20:377–380.
32. Haacke EM, Mittal S, Wu Z, Neelavalli J, Cheng YC. Susceptibility-weighted imaging: technical aspects and clinical applications, part 1. AJNR Am J Neuroradiol 2009;30:19–30.
33. Xu Y, Haacke EM. The role of voxel aspect ratio in determining apparent vascular phase behavior in susceptibility weighted imaging. Magn Reson Imaging 2006;24:155–160.
34. Haacke EM, Brown RW, Thompson MR, Venkatesan R. Magnetic resonance imaging : physical principles and sequence design. New York: Wiley; 1999. xxvii, 914.
35. Haacke EM, Lai S, Reichenbach JR, et al. In vivo measurement of blood oxygen saturation using magnetic resonance imaging: a direct validation of the blood oxygen level-dependent concept in functional brain imaging. Hum Brain Mapp 1997;5:341–346.
36. Fernandez-Seara MA, Techawiboonwong A, Detre JA, Wehrli FW. MR susceptometry for measuring global brain oxygen extraction. Magn Reson Med 2006;55:967–973.
37. Boulot P, Cattaneo A, Taib J, et al. Hematologic values of fetal blood obtained by means of cordocentesis. Fetal Diagn Ther 1993;8:309–316.
38. Schroter B, Chaoui R, Glatzel E, Bollmann R. Normwertkurven fur intrauterine fetale Blutgas- und Saure-Basen-Parameter im 2. und 3. Trimenon. Gynakol Geburtshilfliche Rundsch 1997;37:130–135.
39. Sakhnini L. Magnetic measurements on human erythrocytes: normal, beta thalassemia major, and sickle. J Appl Phys 2003;93:6721–6723.
40. Taylor DS. The magnetic properties of myoglobin and ferrimyoglobin, and their bearing on the problem of the existence of magnetic interactions in hemoglobin. J Am Chem Soc 1939;61:2150–2154.
41. Alpert Y, Banerjee R. Magnetic-susceptibility measurements of deoxygenated hemoglobins and isolated chains. Biochim Biophys Acta 1975;405:144–154.
42. Reichenbach JR, Venkatesan R, Schillinger DJ, Kido DK, Haacke EM. Small vessels in the human brain: MR venography with deoxyhemoglobin as an intrinsic contrast agent. Radiology 1997;204:272–277.
43. Reichenbach JR, Jonetz-Mentzel L, Fitzek C, et al. High-resolution blood oxygen-level dependent MR venography (HRBV): a new technique. Neuroradiology 2001;43:364–369.
44. Brainovich V, Sabatini U, Hagberg GE. Advantages of using multiple-echo image combination and asymmetric triangular phase masking in magnetic resonance venography at 3 T. Magn Reson Imaging 2009;27:23–37.
45. Mok K, Neelavalli J, Liu S, Haacke EM. Susceptibility weighted images using susceptibility maps. In: Proceedings of the 20th Annual Meeting of the ISMRM, Melbourne, Australia, 2012. (abstract 2366).
46. Pisani L, Bammer R, Glover G. Restricted field of view magnetic resonance imaging of a dynamic time series. Magn Reson Med 2007;57:297–307.
47. Wilm BJ, Svensson J, Henning A, Pruessmann KP, Boesiger P, Kollias SS. Reduced field-of-view MRI using outer volume suppression for spinal cord diffusion imaging. Magn Reson Med 2007;57:625–630.
48. Xu Y, Haacke EM. An iterative reconstruction technique for geometric distortion-corrected segmented echo-planar imaging. Magn Reson Imaging 2008;26:1406–1414.
49. Mody S, Yeo L, Neelavalli J, et al. Susceptibility weighted imaging of the fetal brain is superior to ultrasound and conventional MRI sequences in detecting intracranial hemorrhage. In: Abstracts of the 4th International Congress on Fetal MRI, Vienna, Austria, 2013. p 718–730.